

# RSC Advances



This is an *Accepted Manuscript*, which has been through the Royal Society of Chemistry peer review process and has been accepted for publication.

*Accepted Manuscripts* are published online shortly after acceptance, before technical editing, formatting and proof reading. Using this free service, authors can make their results available to the community, in citable form, before we publish the edited article. This *Accepted Manuscript* will be replaced by the edited, formatted and paginated article as soon as this is available.

You can find more information about *Accepted Manuscripts* in the [Information for Authors](#).

Please note that technical editing may introduce minor changes to the text and/or graphics, which may alter content. The journal's standard [Terms & Conditions](#) and the [Ethical guidelines](#) still apply. In no event shall the Royal Society of Chemistry be held responsible for any errors or omissions in this *Accepted Manuscript* or any consequences arising from the use of any information it contains.

# Facile hydrothermal growth of VO<sub>2</sub> nanowire, nanorod and nanosheet arrays as binder free cathode materials for sodium batteries

Hongkuan Wang<sup>a</sup>, Wenzao Li<sup>a</sup>, Huifang Fei<sup>a</sup>, Liping Guo<sup>a</sup>, Jinkui Feng<sup>a,\*</sup>, Lijie Ci<sup>a</sup>,  
Shenglin Xiong<sup>b</sup>

<sup>a</sup> *Key Laboratory for Liquid-Solid Evolution and Processing of Materials (Ministry of Education), School of Material Science and Engineering, Shandong University, Jinan 250061, China*

<sup>b</sup> *School of Chemistry and Chemical Engineering, Shandong University, Jinan 250100, PR China*

## Abstract

Owing to the natural abundance and low standard potential of sodium, Sodium-ion batteries are now considered as promising power systems for electric vehicles and stationary energy storage. Herein, for the first time, we report the synthesis of VO<sub>2</sub> nanowire, nanobelt and nanosheet arrays with preferential (110) orientation on conductive titanium foil by a simple time-dependent hydrothermal method. The morphological and crystallization evolution processes of these products are investigated via XRD, SEM, Raman and TEM in detail. The affection of VO<sub>2</sub> morphology on sodium storage performance is also probed by charge-discharge and EIS. Benefiting from the unique morphology features, The VO<sub>2</sub> nanowire array shows a superior cycle ability of 160 mAh g<sup>-1</sup> after 200 cycles and high rate ability even at 1

---

\*Corresponding author.

E-mail address: [jinkui@sdu.edu.cn](mailto:jinkui@sdu.edu.cn) (J. K. Feng); [lci@sdu.edu.cn](mailto:lci@sdu.edu.cn);

A g<sup>-1</sup>.

**Keywords:** Vanadium dioxide; Array; Cathode materials; Sodium batteries; Hydrothermal

Large-scale applications of electric vehicles and energy storage devices demand high performance and low cost power sources. Li-ion batteries have been the main focus around the world since the first commercialization in 1991 due to their high energy density. However, the high cost and source limitation of lithium-ion battery may restrict its wide applications [1, 2]. The relative abundance of lithium in the Earth's crust is only about 20 ppm. Therefore, it is imperative to seek low-cost alternative that has an abundant reserve. On the other hand, sodium battery has been proposed as a cheap choice because of the geographical distribution of Na (23600 ppm in the Earth's Crust) [3-13].

However, the Na-ion battery (NIB) may not reach the energy level of the Li-ion battery because Na is more than 3 times heavier than Li, the standard electrochemical potential of Na (2.71 V) is lower than Li (3.04 V) with respect to SHE and the lower diffusion rate due to the higher ionic radii of Na<sup>+</sup> to Li<sup>+</sup>. Therefore, searching high capacity and high rate ability electrode materials is urgent and demanding in order to make up for the inherent disadvantages [4].

VO<sub>2</sub> has been regarded as a promising electrode material for LIBs for a long time owing to its high theoretical capacity, low cost, and sufficient supply [14]. In particular, vanadium dioxide stands out because of rapid lithium ion diffusion rate,

higher capacity than other types of vanadium oxides, and its unique VO<sub>2</sub> (B) layer structure formed from edge-sharing VO<sub>6</sub> octahedra [15-25]. Recently, VO<sub>2</sub> was also verified to be a type of high energy cathode materials for NIB (323 mAh g<sup>-1</sup> with the formation of NaVO<sub>2</sub>) compared with Na<sub>0.7</sub>CoO<sub>2</sub>, Na<sub>0.44</sub>MnO<sub>2</sub> and Na<sub>3</sub>V<sub>2</sub>(PO<sub>4</sub>)<sub>3</sub> et al [4,26,27]. Nevertheless, it is worth noting that the application of VO<sub>2</sub> in practical NIBs is seriously impeded by the poor capacity retention due to large volume expansion/contraction (NaVO<sub>2</sub>/VO<sub>2</sub> = 150%) during the sodium intercalation and de-intercalation reactions between sodium ion and VO<sub>2</sub>. The repeated processes result in pulverization of the electrodes and finally destroy the initial structure. Tailored nanoarchitecture design and additional surface engineering of active materials are desirable, which can both secure high surface conductivity and ensure the structure integrity for long-time and high-rate cycling. For example, in 2014, Jiao et al. first reported the sodium storage of single crystalline VO<sub>2</sub> nanosheets, the nanosheets electrode delivered a high capacity retention [26]. Then Chao et al. reported the sodium storage of single-crystalline VO<sub>2</sub> nanobelts array on graphene network, the capacity retentions greatly improved by graphene quantum dots coating layer [27].

Recently, several studies have revealed that Li-ion and Na-ion diffusion are associated with their particle size and morphology [28-39]. Meanwhile, the array structure may form percolation pathways via the opening of active diffusion channels that could potentially facilitate ionic diffusion [28, 38]. For example, Liu and Lou reported that lithium diffusion can be facile in nanoarray structure due to abundant diffusion channels, suggesting that the design of morphology could supply high capacity and

high energy density [28]. Cao et al. reported that amorphous  $V_2O_5$  demonstrated superior electrochemical properties upon sodiation in comparison with its crystalline counterpart by demonstrating the capacity twice than crystalline  $V_2O_5$  with a much higher discharge potential, energy density, and cycle stability [38]. It has been verified by many groups that the structure design could exhibit outstanding cycling stability and rate performance compared with the cathodes [30-35]. Besides that, we found that time dependent synthesis of  $Zn_2GeO_4$  could result in quite different lithium storage character [39].

It is worthy to investigate morphology affection on the sodium storage performance of  $VO_2$  as their isotropic characteristics may enhance Na-ion diffusion by offering diffusion paths, which are short and not highly anisotropic. In this paper, we demonstrate our tailored  $VO_2$  nanostructured array on titanium metal substrate as the cathode for NIBs. It is found that by simply changing the reaction time,  $VO_2$  nanowire, nanobelt and nanosheet arrays are obtained. Moreover, it is found that the degree of crystallinity is also time dependent. The open space between the arrays not only allows steady diffusion of electrolyte and sodium ion, but also buffer the volume changes and prevent the capacity loss. The nanowire arrays synthesized in 40 min show a low crystalline character, which makes themselves become more anisotropic and provides more potential defects, thus promoting the arrays' electrochemical performance. When used as cathode materials for NIBs, the low crystallized nanowire array structures exhibit superior electrochemical performance of best cycle abilities, and high rate capabilities in comparison with  $VO_2$  nanobelt and nanosheet arrays on

Ti foil. All in all, the present crystallized nanowire arrays are promising candidates as cathode materials for NIBs.

### **Experimental section**

Ammonium metavanadate ( $\text{NH}_4\text{VO}_3$ , 99%) and Oxalic acid ( $\text{H}_2\text{C}_2\text{O}_4 \cdot 2\text{H}_2\text{O}$ , 99%) were purchased from Sinoreagent Corp. Both of the chemicals were used without further purification. In a typical procedure as shown in Figure 1, 4 mmol  $\text{NH}_4\text{VO}_3$  and 4.8 mmol  $\text{H}_2\text{C}_2\text{O}_4 \cdot 2\text{H}_2\text{O}$  were added into 80 mL distilled water. After magnetic stirring for 15 min, the yellowish green solution was obtained, and then transferred into 100 mL Teflon-lined stainless steel autoclave liners with titanium foil which was washed with ethanol and 2 M HCl in order and coated with polytetrafluoroethylene tape on one side to avoid solution contamination. The autoclave was maintained at 180 °C for 40min, 2h and 12h respectively, and then cooled to room temperature naturally. The resulting samples were cleaned with distilled water several times and dried at 60 °C for 10 h.

### **Characterization**

The prepared samples were characterized by powder XRD (Rigaku Dmaxrc diffractometer,  $V = 50 \text{ kV}$ ,  $I = 100 \text{ mA}$ ) at a scanning rate of  $5 \text{ degree min}^{-1}$ . The morphologies and structures were observed by field-emission scanning microscopy (FE-SEM, JSM-6700F, JEOL) and TEM/HR-TEM (JEM-2100F (JEOL)). To further understand structure of the samples, we investigate the samples by Raman Spectroscopy on a Horiba Jobin-YVON co-focal laser Raman system with He-Ne 632 nm laser as the excitation source.

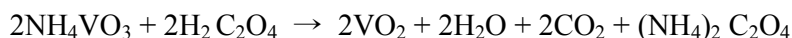
### Electrochemical Measurement

The electrochemical performance was examined in 2016-type coin cells, assembled in an Ar-filled dry glove box with both the moisture and oxygen content below 1 ppm. The VO<sub>2</sub>@Ti foil was used directly without any binder or additive. For sodium-ion battery fabrication, the metallic sodium foil as the counter-electrode, 1 M NaPF<sub>6</sub> in ethylene carbonate (EC)-diethyl carbonate (DEC)-fluoroethylene carbonate (FEC) (1:1:0.05 in volume) as the electrolyte, and glass fiber as the separator. Galvanostatic discharge-charge measurements of the cells were carried out in a voltage range of 1.5-3.8 V at various rates. Cyclic voltammetry (CV) tests were performed at a scanning rate of 0.1 mV s<sup>-1</sup> between 1.5 and 3.8 V (vs. Na/Na<sup>+</sup>).

### Results and discussions

The as-prepared VO<sub>2</sub> arrays are in black color (S1). The crystal structures of the samples are examined by X-ray diffraction (XRD). Figure 2a shows powder XRD patterns of the samples synthesized after different reaction times with the standard VO<sub>2</sub> and Ti substrate patterns, respectively. All the diffraction peaks could be assigned perfectly to the metaphase monoclinic VO<sub>2</sub>(B) (space group. C2/m) structure (JCPDS Card No. 65-7960) and Ti substrate (JCPDS Card No.65-3362). No other impure peaks were observed. It displays a partially crystalline structure with (110) preferred orientation at 2θ=26°, and two minor peaks at 2θ=47.1° and 47.5°, corresponding to the (020) and (312) reflections, respectively [26,27]. With the increasing hydrothermal time, the XRD intensity of the VO<sub>2</sub> became stronger, indicating that the crystallinity of the VO<sub>2</sub> is gradually improved. The VO<sub>2</sub> array was further

characterized by Raman spectra, as shown in Figure 2b. Generally, all VO<sub>2</sub> samples display similar spectrum. The analysis of the spectra exhibits well defined bands centered at around 148, 280, 408, 506, 691 cm<sup>-1</sup>. These bands can be assigned to the fundamental modes of crystalline VO<sub>2</sub> (B) monoclinic structure. The predominant low-wave number bond at 148 cm<sup>-1</sup> is attributed to the skeleton bent vibration of (V<sub>2</sub>O<sub>2</sub>)<sub>n</sub>, which is a characteristic of VO<sub>2</sub>. The bands located at 280 and 408 cm<sup>-1</sup> are assigned to the bending vibration of the V=O double bonds. The band at 506 cm<sup>-1</sup> is attributed to the triply-coordinated oxygen (V<sub>3</sub>-O) stretching mode. The band at 691 cm<sup>-1</sup> is assigned to the stretching vibration of the doubly coordinated oxygen (V<sub>2</sub>-O). The results are corresponding well with the previous report [27]. The total reaction could be proposed as follow:



Field-emission scanning electron microscopy (FESEM) images of the as-obtained samples, including the panoramic and locally enlarged FESEM images of VO<sub>2</sub> arrays (Figure 3) at different reaction time. In our synthesis process, the morphological evolution of VO<sub>2</sub> was found to depend strongly on reaction time [27]. For instance, our time-dependent experiments in Figure 3 show that the morphology of the precursor evolves significantly at the elevated reaction time. Within the first 40 min, dense thin needle arrays were formed. Titanium foil turned from pristine grey to black as observed by the eye, which showed that VO<sub>2</sub> had formed at this time. As the reaction proceeded, the shape of the product was gradually transformed from crossed nanowire arrays to nanobelt arrays after 2 h and finally to nanosheet arrays after 12 h.

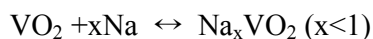
Hence the array formation is a gradual crystallization self-assembly process via wall-like direction. A gradual crystallization self-assembly process is proposed as indicated by our previous work [37,38]. Indeed, the deeper formation mechanism needs to be studied in the future. The EDX (Figure S1) could confirm the existence of V and O elements.

The diameter and height of the as-prepared array observed by FESEM and TEM are 50-200 nm and 4-8  $\mu\text{m}$ , respectively. From the enlarged side-view FESEM and TEM images, it can be observed that each array is composed of numerous curve and bend, which may increase the surface area and facilitate the sodium ion diffusion. The high-resolution TEM (Figure 4d) suggests that the  $\text{VO}_2$  nanosheet is composed of discontinuous crystalline and amorphous domains. The lattice fringe of the crystalline domain is 0.352 nm, which can be assigned to the (110) plane. The result is in good agreement with monoclinic  $\text{VO}_2$  (B) as confirmed by XRD [26-27]. The selected-area electron diffraction (SAED) pattern (inset) was taken from the individual nanowire region of Figure 4b, demonstrating that the synthesized nanowires are low crystallized.

To examine the sodium storage performances of the obtained products, different nanostructured  $\text{VO}_2$  arrays were fabricated as cathodes and assembled in coin type cells. The long cycling performances of three samples were performed at the rate of  $0.3 \text{ A g}^{-1}$ . From the Figure 5a, we can see that all the three samples show capacity increase at initial cycles probably due to an activation process. Then the capacity slowly decreased. Among them, the  $\text{VO}_2$  nanowire array showed the best cycling

ability, which remained about  $160 \text{ mAh g}^{-1}$  even after 200 cycles. In contrast, for the other two morphologies of  $\text{VO}_2$ , the capacity retention is only about  $89 \text{ mAh g}^{-1}$  for 2 h and  $76 \text{ mAh g}^{-1}$  for 12 h samples, respectively. The longer cycling performance may result from the unique morphological, crystalline structure and surface area, which could accommodate the volume changes and expedite the charge transfer process. The 1<sup>st</sup>, 2<sup>nd</sup>, 100<sup>th</sup> and 200<sup>th</sup> charge-discharge curves of  $\text{VO}_2$  array are also given in Figure 5b. The curves show two main slopes plateau which is consistent with the CV results. As expected, the  $\text{VO}_2$  nanowire array electrode also exhibits good rate capacity, as shown in Figure 5c. It delivered a reversible capacity of  $180 \text{ mAh g}^{-1}$  at  $0.1 \text{ A g}^{-1}$ ,  $160 \text{ mAh g}^{-1}$  at  $0.3 \text{ A g}^{-1}$ ,  $150 \text{ mAh g}^{-1}$  at  $0.4 \text{ A g}^{-1}$ ,  $120 \text{ mAh g}^{-1}$  at  $0.6 \text{ A g}^{-1}$ . Even at high rate of  $1 \text{ A g}^{-1}$ , the reversible capacity maintained approximately  $90 \text{ mAh g}^{-1}$ . Moreover, when the rate turns back to  $0.25 \text{ A g}^{-1}$ , the capacity can retain as high as  $179 \text{ mAh g}^{-1}$ . These results suggest that the structure of the  $\text{VO}_2$  array composite electrode achieves extraordinary stability even under high rate long-cycling and this is very critical for potential applications. To further understand the electrochemical performance of the  $\text{VO}_2$  array electrode, cyclic voltammetry (CV) scans were carried out at a sweeping rate of  $0.1 \text{ mV/s}$  in the voltage window from 1.5 to 3.8 V versus  $\text{Na/Na}^+$ . As Figure 5d shows, during the first cathodic scan, several broad reduction peaks occurred from 2.8 to 1.5 V. The sequential cathodic peaks may be ascribed to the sodium ion intercalation processes from successive  $\text{VO}_2$  reduction reactions [21,22]. In the first anodic scan, one peak appeared and should be ascribed to the desodiation process. When the cycling number increases, the anodic and cathodic areas come to

almost equal in size, suggesting a more reversible sodiation/de-sodiation reaction [26,27]. The reaction mechanism could be concluded as:



The detailed mechanism needs further research clarification.

To better understand the stability difference of VO<sub>2</sub> electrodes, we investigate the morphology of electrode removed from cells after 200 cycles via ex-situ SEM imaging. As evidently exhibited in Figure 6, the morphology of the 40 min-grown arrays retained best after 200 cycles. However, for the 2 h and 12 h samples, slightly aggregation and distortion are observed, which may affect the connection between the active materials and electrolyte. The less morphology change of 40 min sample may be ascribed to its higher surface area and thinner wall thickness. This morphological change during cycling is a possible reason of capacity fading [40-44].

To further understand the different cycling performance of different nanostructured VO<sub>2</sub> arrays, electrochemical impedance spectroscopy (EIS) studies (Figure 7) were carried out by using the cycled VO<sub>2</sub> array/Na half-cell to study the kinetic mechanisms of Na storage, as presented in Figure 7. The Nyquist-plots were recorded at a frequency range of 0.01 Hz-100 kHz at amplitude of 5 mV. In the EIS study, the VO<sub>2</sub> array electrodes were used as working electrodes and sodium foils as both anode and reference electrodes. The results are typically Nyquist plots with one compressed semicircle at high frequency and a straight line at low frequency [40-44]. The semicircle is believed to be attributed to the surface film impedance in the high frequency and the charge transfer resistance in the middle frequency. From the Figure

7, we can see that the total resistances of the 40 min prepared electrode (2600  $\Omega$ ) are much smaller than the 2 h and 12 h electrodes (5000, 7000  $\Omega$ ). These results were consistent well with the electrochemical performance and further proved that the 40 min-prepared VO<sub>2</sub> array has a lower charge transfer performance [44].

### Conclusions

In this work, we present a facile one-pot hydrothermal route to prepare various structured VO<sub>2</sub> arrays assembled from primary building units of ultrathin nanowires on titanium foil with strong adhesion for the first time. It is discovered that the reaction time plays a crucial role on the morphology of VO<sub>2</sub>. The nanowire array structure shows the best sodium storage performance. Both the Ex-situ SEM and EIS reveal that the low crystalline property, array structure and surface area can account for the superior electrochemical performance.

### Acknowledgement

This work was supported by Key Research Plan of Shandong Province (2015GGE27286), the National Natural Science Foundation of China (Grant No.21203110) (No. 21371108) , Independent Innovation Foundation of Shandong University (No.2012ZD008), Shandong Provincial Natural Science Foundation for Distinguished Young Scholar, the National Natural Science Funds for Distinguished Young Scholars (Grant no. 51025211) and China Postdoctoral Science Foundation (No. 2013M541903).

### References:

- [1] P. Poizot, S. Laruelle, S. Grugeon, L. Dupont, J. M. Tarascon, *Nature* 407 (2000) 496.
- [2] J.M. Tarascon, *Nat. Chem.* 2 (2010) 510.
- [3] D. Kundu, E. Talaie, V. Duffort, L.F. Nazar, *Angew. Chem. Int. Ed.* 54 (2015) 3431-3448.
- [4] N. Yabuuchi, K. Kubota, M. Dahbi, S. Komaba, *Chem. Rev.* 114 (2014) 11636-11682.
- [5] H. Kim, J. Hong, K. Park, H. Kim, S.W. Kim, K Kang, *Chem. Rev.* 114 (2014) 11788-11827.
- [6] Y.J. Fang, L.F. Xiao, J.F. Qian, X.P. Ai, H.X. Yang, Y.L. Cao, *Nano Lett.* 14 (2014) 3539-3543.
- [7] C.J. Chen, Y.W. Wen, X. L. Hu, X.L. Ji, M.Y. Yan, L.Q. Mai, P. Hu, B. Shan, Y.H. Huang, *Nature Comm.* 6 (2015) 6929.
- [8] W.S. Wang, R.J. Xiao, Y.S. Hu, M. Avdeev, L.Q. Chen, *Nat. Commun.* 6 (2015) 6954.
- [9] J.Y. Hwang, S.M. Oh, S.T. Myung, K.Y. Chung, I. Belharouak, Y.K. Sun, *Nat. Commun.* 6 (2015) 6865.
- [10] P. Barpanda, G. Oyama, S. Nishimura, S. Chung, A. Yamada, *Nat. Commun.* 5 (2014) 4358.
- [11] D.D. Yuan, X.M. Liang, L. Wu, Y.L. Cao, X.P. Ai, J.W. Feng, H.X. Yang, *Adv. Mater.* 26 (2014) 6301-6306.
- [12] Y.L. Cao, L.F. Xiao, W. Wang, D.W. Choi, Z.M. Nie, J.G. Yu, L.V. Saraf, Z.G.

- Yang, J. Liu, *Adv. Mater.* 23 (2011) 3155-3160.
- [13] H. Li, X.Q. Yu, Y. Bai, F. Wu, C. Wu, L.Y. Liu, X.Q. Yang, *J. Mater. Chem. A* 3 (2015) 9578-9586.
- [14] C.Z. Wu, F. Feng, Y. Xie, *Chem. Soc. Rev.* 42(2013) 5157-5183.
- [15] M. V. Reddy, G. V. Subba Rao, B. V. R. Chowdari, *Chem. Rev.* 113 (2013) 5364-5457.
- [16] L.Q. Mai, X.C. Tian, X. Xu, L. Chang, L. Xu, *Chem. Rev.* 114 (2014) 11828-11862.
- [17] N. A. Chernova, M. Roppolo, A. C. Dillon, M.S. Whittingham, *J. Mater. Chem.* 19 (2009) 2526-2552.
- [18] G.S. Zakharova, V.L. Volkov, *Russ. Chem. Rev.* 72 (2003) 311-325.
- [19] H. Heinz, *Clay Miner.* 7 (2012) 205-230.
- [20] C.J. Niu, J.S. Meng, C.H. Han, K.N. Zhao, M.Y. Yan, L.Q. Mai, *Nano Lett.* 14 (2014) 2873-2878.
- [21] A.Q. Pan, H.B. Wu, L. Yu, X. W. D. Lou, *Angew. Chem. Int. Ed.* 52 (2013) 2226-2230.
- [22] M. Lee, B.H. Wee, J.D. Hong, *Adv. Energy Mater.* 5 (2015) 1401890.
- [23] J.M. Won, Y.N. Ko, J.K. Lee, Y.C. Kang, *Electrochim. Acta* 156 (2015) 179-187.
- [24] S. Yang, Y. Gong, Z. Liu, L. Zhan, D. P. Hashim, L. Ma, R. Vajtai and P. M. Ajayan, *Nano Lett.* 13 (2013) 1596-1601.
- [25] G.F. Ren, M.N.F. Hoque, X. Pan, J. Warzywoda, Z.Y. Fan, *J. Mater. Chem. A* 3 (2015) 10787-10794.

- [26] M. Ogawa, K. Kuroda, *Chem. Rev.* 95(1995) 399-438.
- [27] D. Chao, C. Zhu, X. Xia, J. Liu, X. Zhang, J. Wang, P. Liang, J. Lin, H. Zhang, Z. Shen and H. J. Fan, *Nano Lett.* 15 (2015) 565-573.
- [28] J. Jiang, Y.Y. Li, J.P. Liu, X.T. Huang, C.Z. Yuan, X.W. Lou, *Adv. Mater.* 24 (2012) 5166-5180.
- [29] E. Uchaker, Y. Z. Zheng, S. Li, S. L. Candelaria, S. Hu and G. Z. Cao, *J. Mater. Chem. A* 2 (2014) 18208-18214.
- [30] X. Tang, B.H. Lin, Y. Ge, Y. Ge, C.J. Lu, S.V. Savilov, S.M. Aldoshin, H.Xia, *Mater. Res. Bull.* 69 (2015) 2-6.
- [31] Y.J. Fang, L.F. Xiao, J.F. Qian, X.P. Ai, H.X. Yang, Y.L. Cao, *Nano Lett.* 4 (2014) 3539-3543.
- [32] H. Sohn, M.L. Gordin, M. Regula, D.H. Kim, Y.S. Jung, J.X. Song, D.H. Wang, *J. Power Sources* 302 (2016) 70-78.
- [33] H. Xia, Y.H. Wan, W. Assenmacher, W. Mader, G.L. Yuan, L. Lu, *NPG Asia Mater.* 6 (2014) e126.
- [34] S. Yang, B.G. Yan, T. Li, J. Zhu, L. Lu, K.Y. Zeng, *Phys. Chem. Chem. Phys.* 17 (2015) 22235-22242.
- [35] H. Xia, L. Lu, G. Ceder, *J. Power Sources* 159 (2006) 1422-1427.
- [36] L.W. Zhao, J.F. Ni, H.B. Wang, L.J. Gao, *RSC Adv.* 3 (2013) 6650-6655.
- [37] J.F. Qian, X.Y. Wu, Y.L. Cao, X.P. Ai, H.X. Yang, *Angew. Chem. Int. Ed.* 52 (2013) 4633-4636.
- [38] C. Li, X. Miao, W. Chu, P. Wu, D.G. Tong, *J. Mater. Chem. A* 3 (2015)

8265-8271.

[39] R. Yi, J.K. Feng, D.P. Lv, M.L. Gordin, S.R. Chen, D.W. Choi, D.H. Wang, *Nano Energy* 2 (2013) 498–504.

[40] Y. Wang, H. Xia, L. Lu, J.Y. Lin, *ACS Nano* 4 (2010) 1425-1432.

[41] J.C. Liu, Y.J. Xu, X.J. Ma, J.K. Feng, Y.T. Qian, S.L. Xiong, *Nano Energy* 7 (2014) 52-62.

[42] F.F. Wu, X.J. Ma, J.K. Feng, Y.T. Qian, S.L. Xiong, *J. Mater. Chem. A* 2 (2014) 11597-11605.

[43] F. Zhang, R.H. Zhang, J.K. Feng, L.J. Ci, S.L. Xiong, J. Yang, Y.T. Qian, L.F. Li, *Nanoscale* 7 (2015) 232-239.

[44] S. Liu, J.K. Feng, X.F. Bian, Y.T. Qian, J. Liu, H. Xu, *Nano Energy* 13 (2015) 861-897.

**Figure Captions :**

Figure 1. Schematic illustration for the preparation of vanadium oxide arrays on Ti foil.

Figure 2. (a) XRD patterns and (b) Raman spectrums of the as-grown VO<sub>2</sub> nanostructures on Ti foil at reaction time of 40 min, 2 h and 12 h.

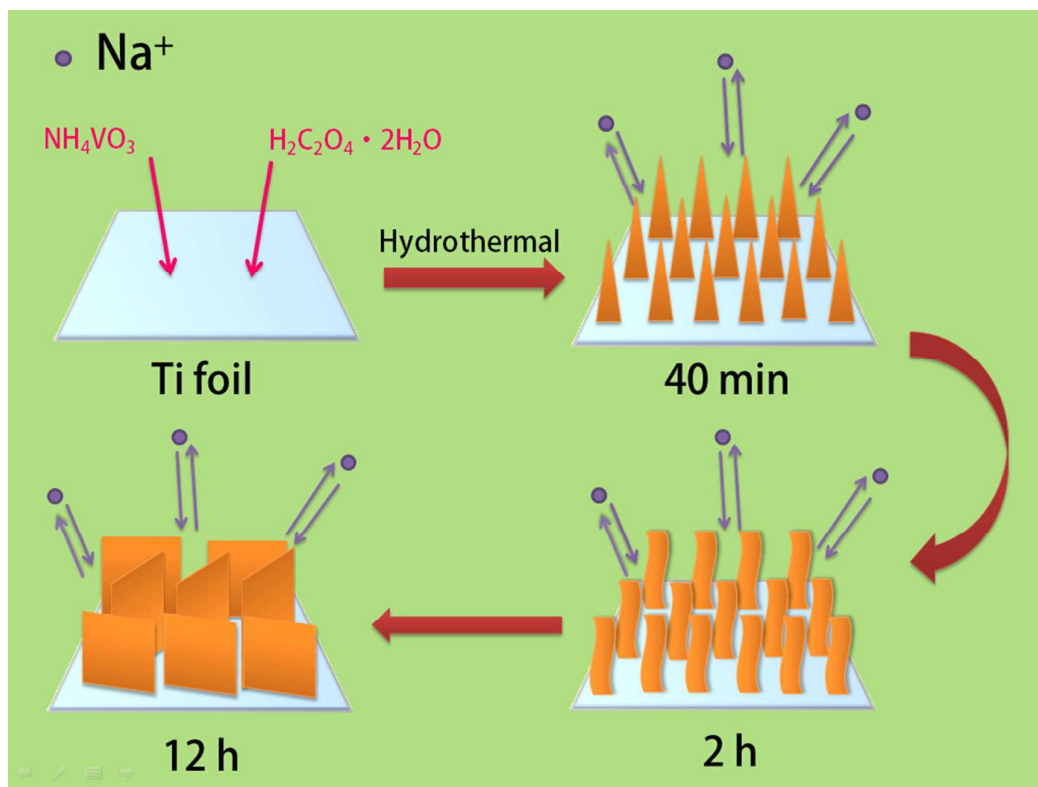
Figure 3. Structural evolution of the corresponding VO<sub>2</sub> arrays assembled on Ti foil at different reaction time (FESEM images): 40 min (a and b), 2 h (c and d) and 24 h (e and f).

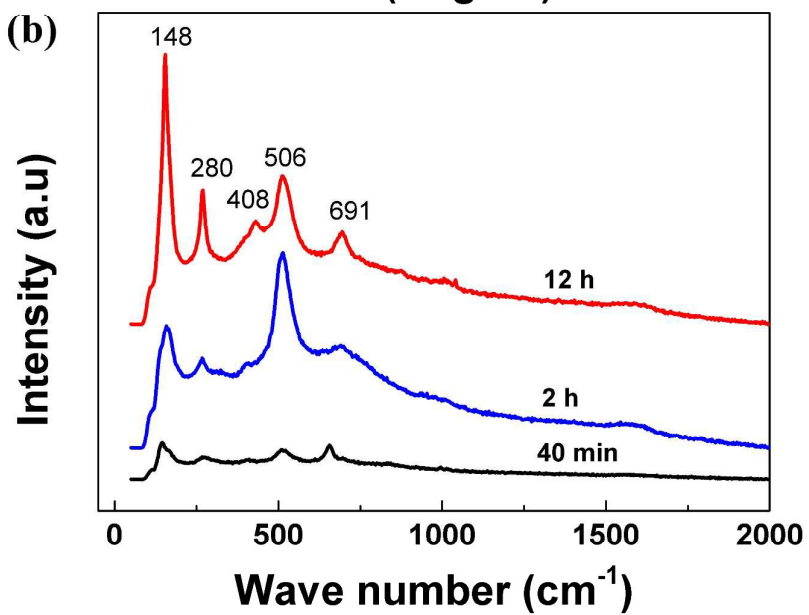
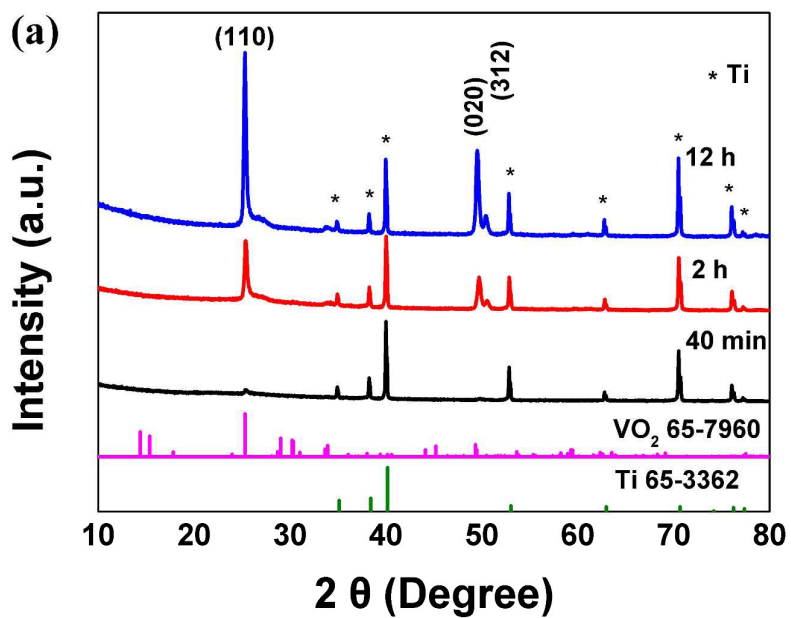
Figure 4. (a) Top-view and (b) side-view SEM images (c) TEM and (d) HRTEM images of VO<sub>2</sub> array on Ti foil at the reaction time of 2 h.

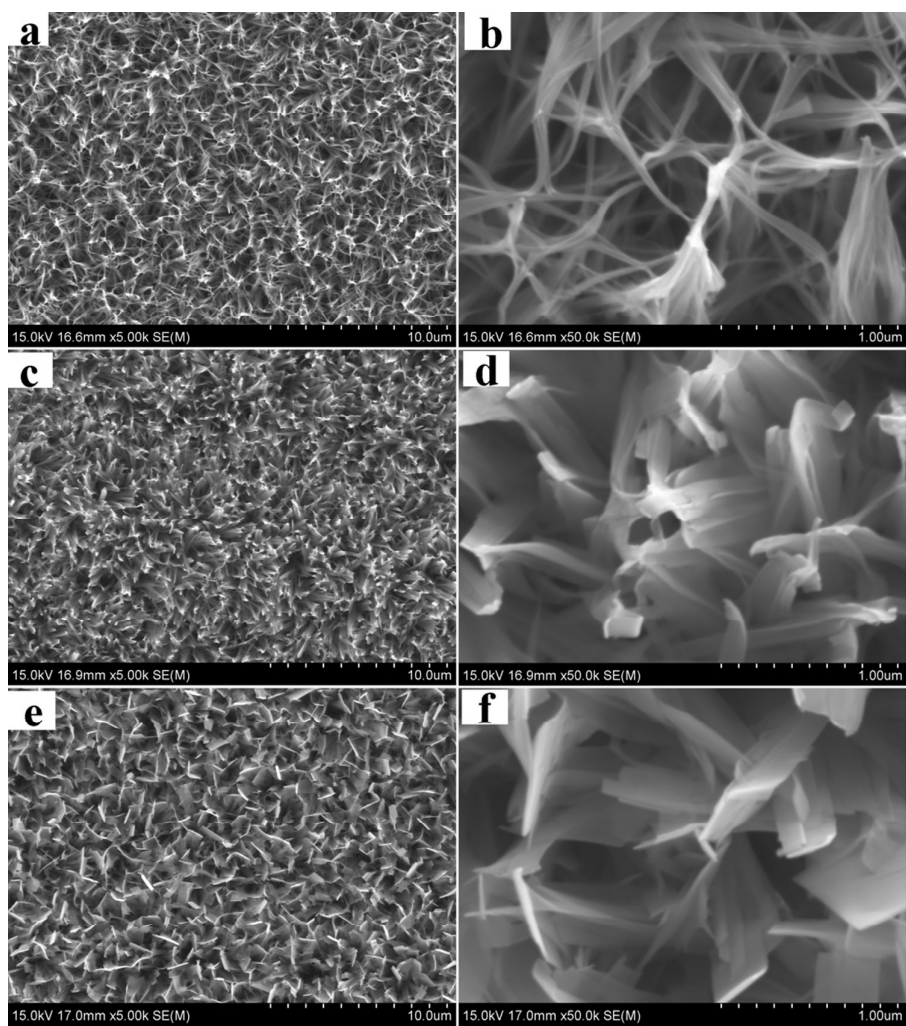
Figure 5. (a) Cycling of VO<sub>2</sub> array at a current of 0.3 A g<sup>-1</sup> at different reaction time. (b) Charge–discharge curves of VO<sub>2</sub> array at a current density of 0.3 A g<sup>-1</sup>. (d) Rate capability of VO<sub>2</sub> at various current densities. (d) The first three consecutive cyclic voltammetry (CV) curves for the VO<sub>2</sub> array at a scan rate of 0.1 mV s<sup>-1</sup> in the voltage window of 1.5–3.8 V (vs. Na/Na<sup>+</sup>).

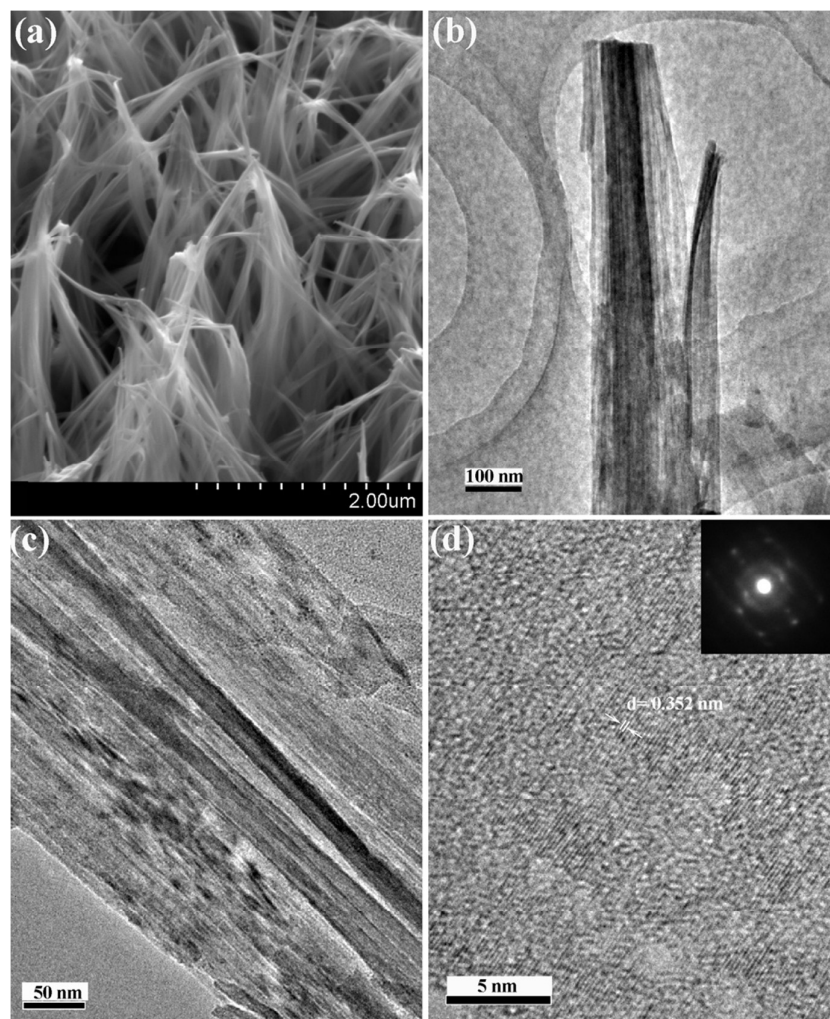
Figure 6. The ex-situ SEM images of the 200<sup>th</sup> cycled at different reaction time (FE-SEM images): 40 min (a and b), 2 h (c and d) and 12 h (e and f).

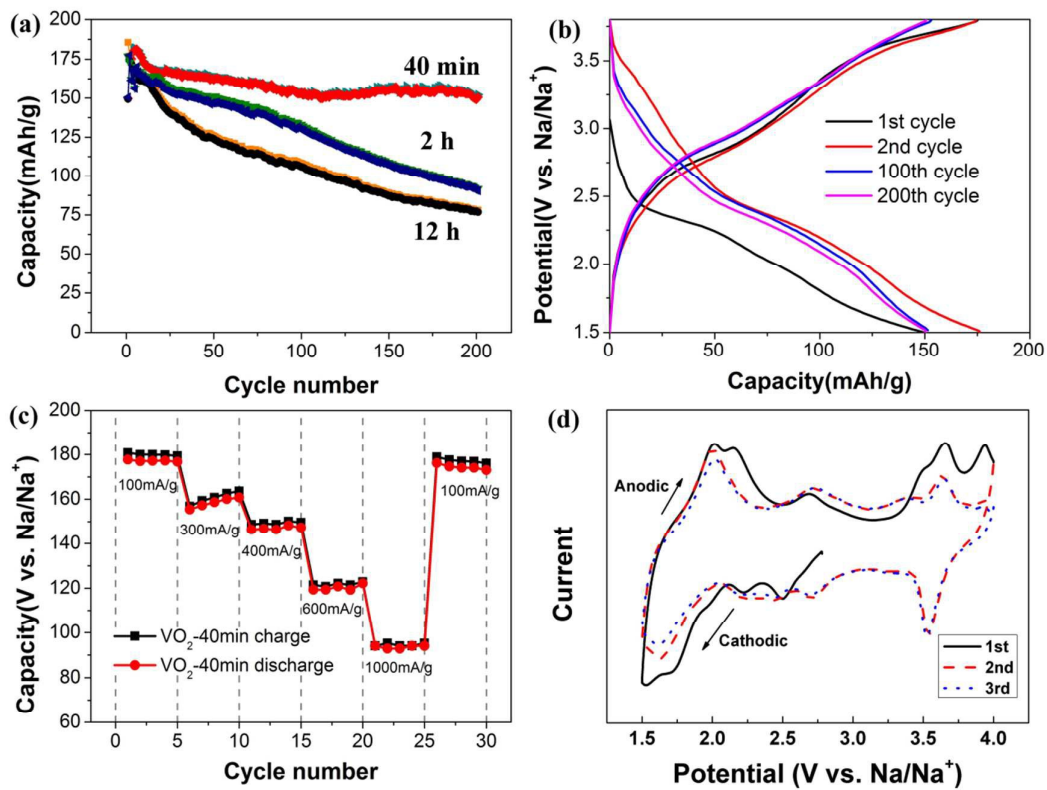
Figure 7. Nyquist plots of cycled VO<sub>2</sub> array/Na cell at different reaction time.

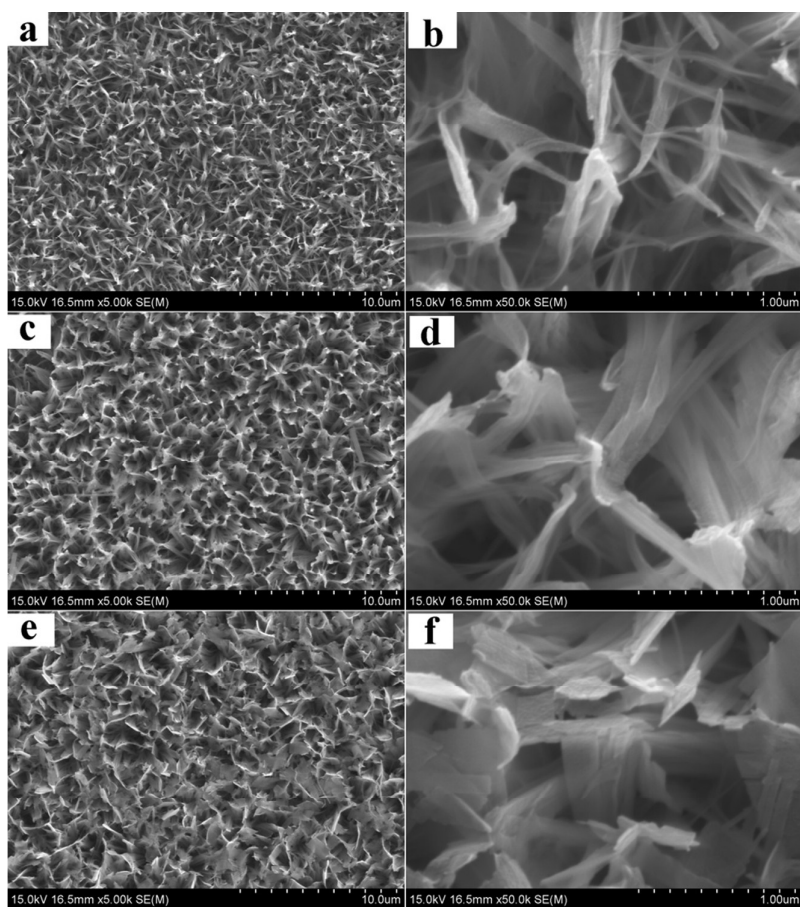


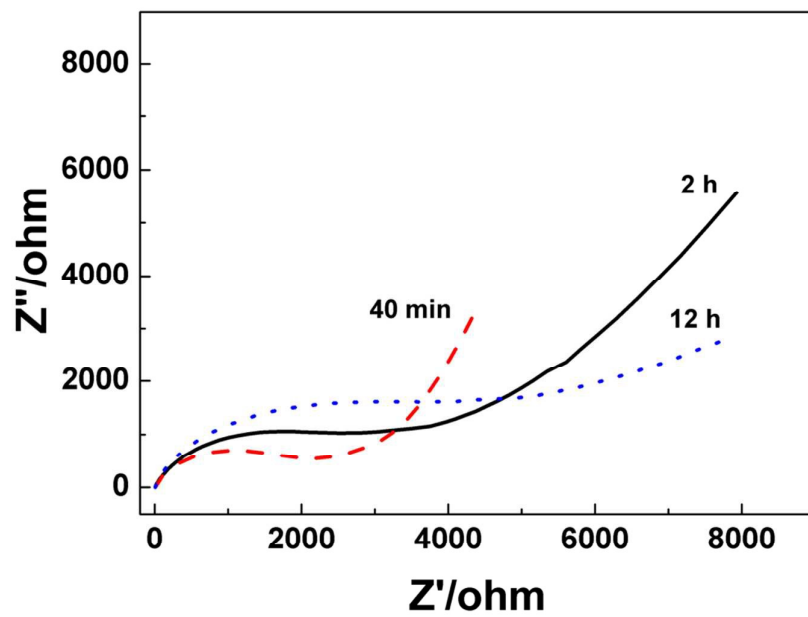


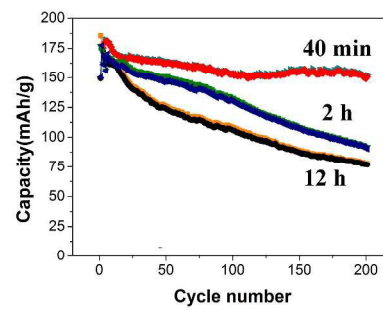
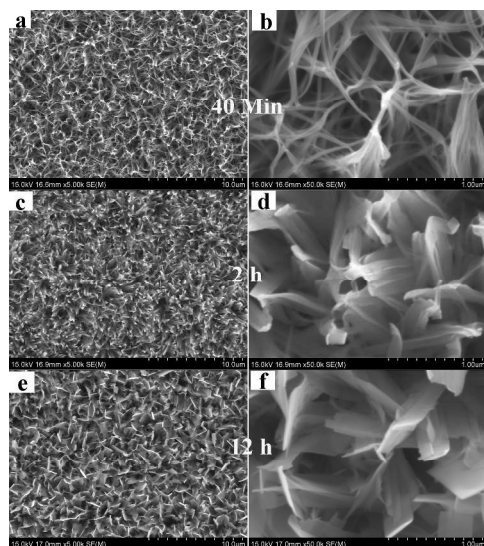












533x287mm (300 x 300 DPI)